1 Results

The results of the numerical experiments will be presented in this chapter. For both optimization targets the optimized pulses, their properties and the final evolved state will be presented.

1.1 Qubit state transfers

1.1.1 $|0\rangle \rightarrow |1\rangle$ state transfer

In fig. 1.1 the fidelity during all optimization runs are plotted. For pulse lengths longer than 15 ns the fidelity starts at values close to the goal ($F > 0.9$) and the number of iterations is relatively low (less than 85 iterations). In contrast, pulses shorter than 15 ns start at lower fidelities while the number of iterations are roughly one order of magnitude larger with no clear pattern with respect to the pulse length.

To give a more detailed picture, the starting fidelity and optimized fidelity is plotted over pulse length in fig. 1.2. The optimizations where the fidelity goal was not reached, pulse lengths equal to and below 10.50 ns, are marked with stars.

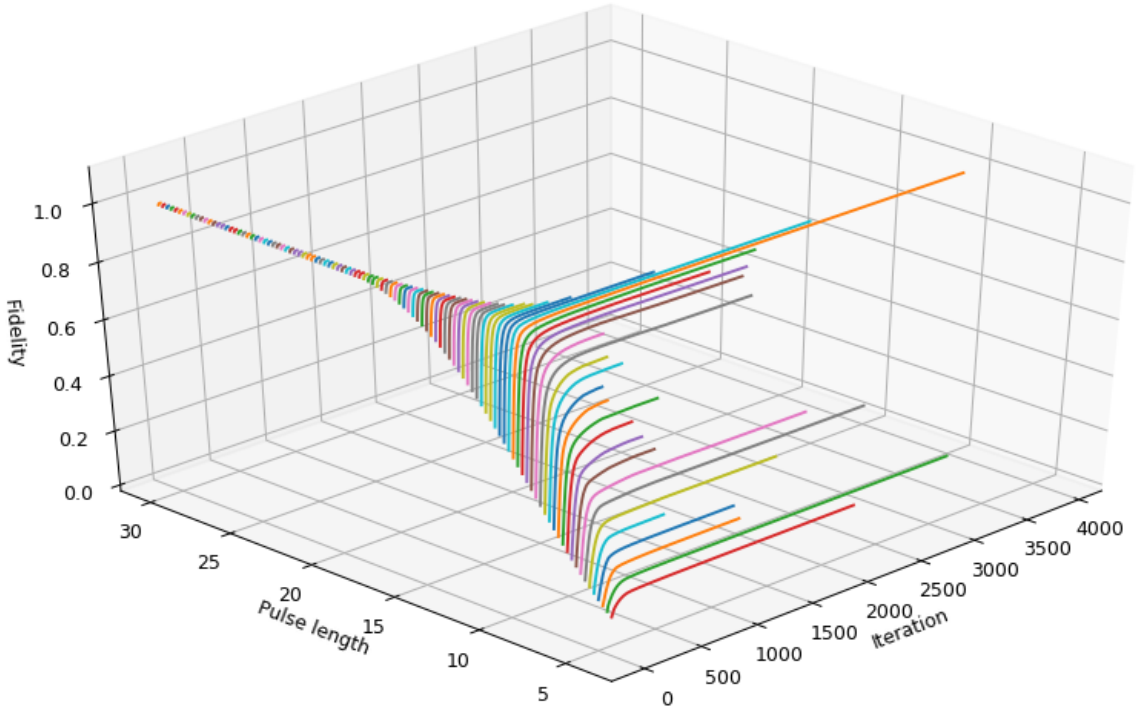

Figure 1.1: Fidelity during optimizations for every pulse length (ns). The different colors help distinguish the lines.

Further analysis is done on pulses with lengths 4.25 ns, 6.0 ns, 8.0 ns, 10.0 ns, 20.0 ns and 30.0 ns. The optimized pulse shapes $\mathrm{Re}(\Omega)$ and $\mathrm{Im}(\Omega)$ are plotted in fig. 1.3 together with the guess pulses. Pulses longer than 20 ns require only fine adjustments to the Blackman guess pulse while shorter pulses have an imaginary part which is maximized for the whole duration of the pulse.

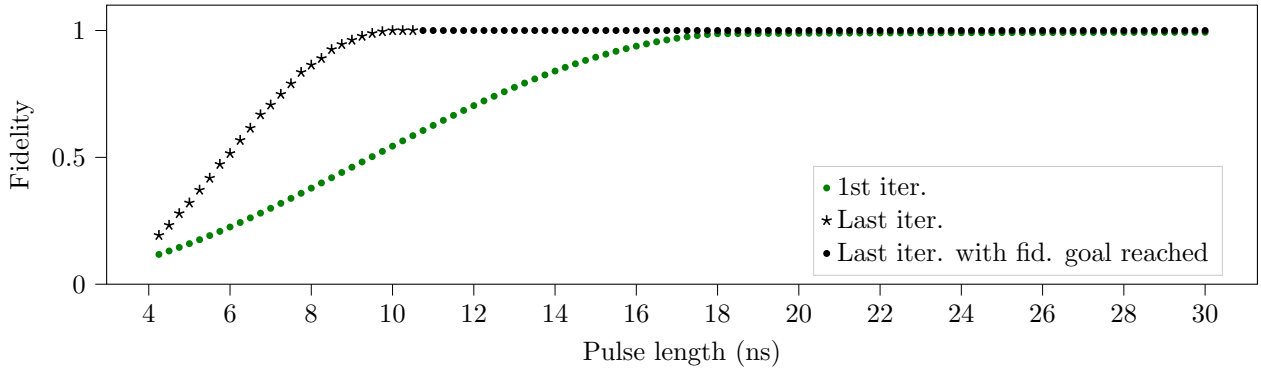

Figure 1.2: Fidelity of first and last iteration of every pulse length.

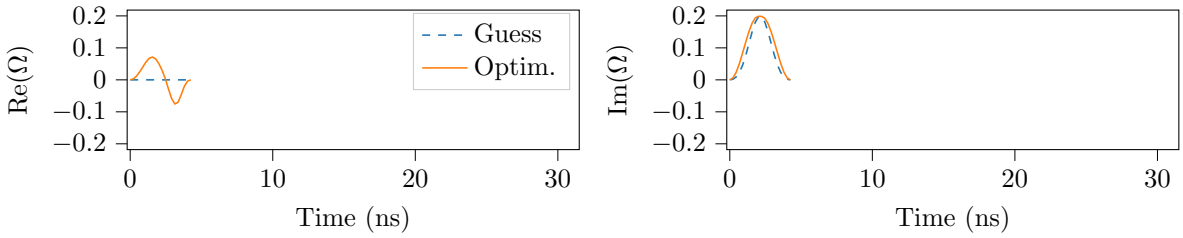

(a) Pulse length 4.25 ns

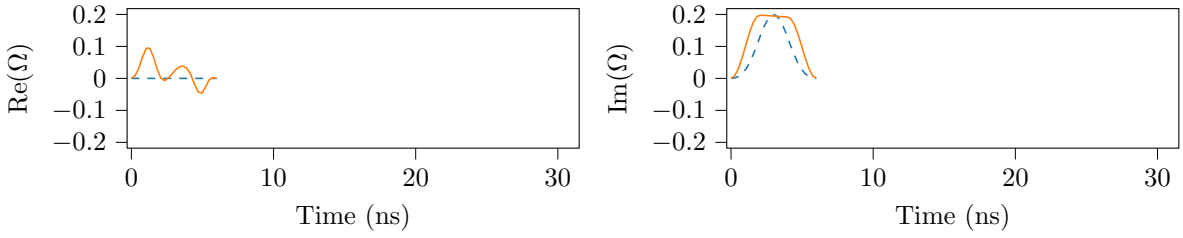

(b) Pulse length 6.0 ns

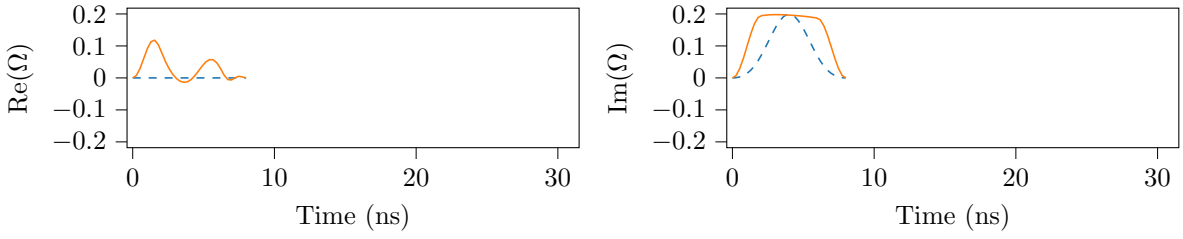

(c) Pulse length 8.0 ns

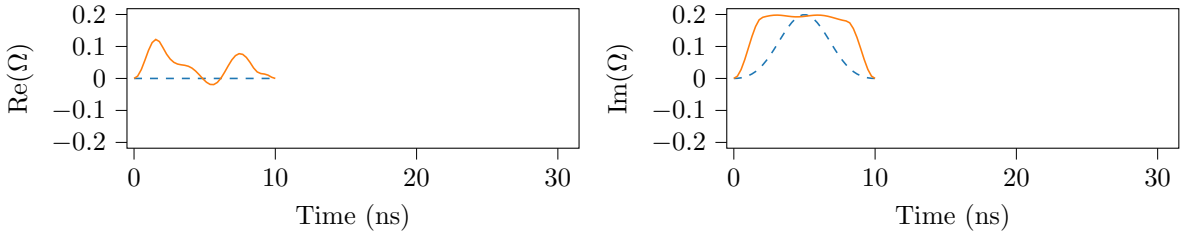

(d) Pulse length 10.0 ns

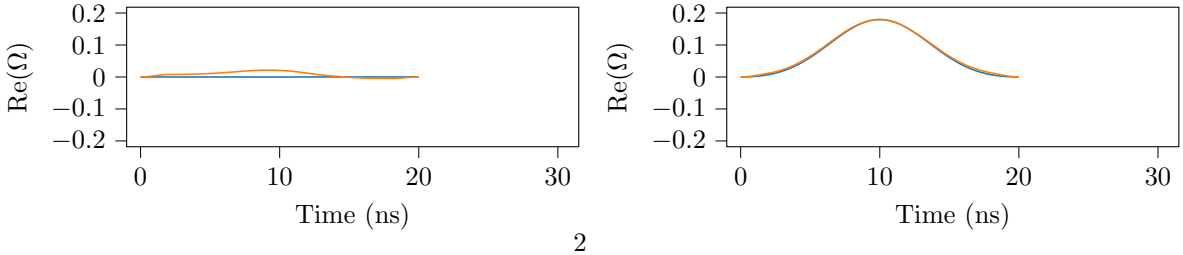

(e) Pulse length 20.0 ns

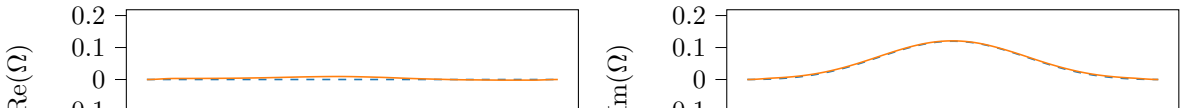

The spectrum of $\Omega(t)$ in the lab frame ($\Omega(t)e^{i\omega_q t}$) is shown in fig. 1.4. For all pulse lengths there is a peak centered roughly at ω_q with a quickly decaying end in positive direction (towards $\omega_q + \kappa_q$). Following the trend, it can be observed that the width of the peak becomes narrower for longer pulses. For the highest pulse length 30 ns there is almost no support at $\omega_q + \kappa_q$ nor $\omega_q - \kappa_q$.

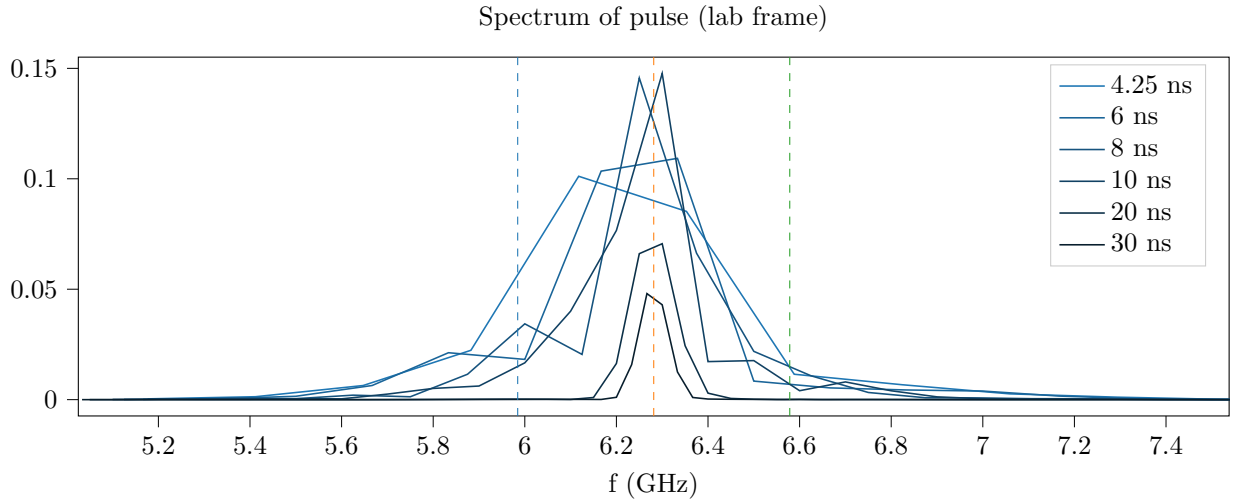

Figure 1.4: Frequency spectrum of the complex pulses in fig. 1.3. The vertical lines indicate (from left to right) $\omega_q - \kappa_q$, ω_q, $\omega_q + \kappa_q$ (all divided by 2π).

The time evolution of the system under the optimized pulses are visualized by plotting the occupation of the states over time, fig. 1.5, and the projection of the state on the Bloch sphere over time, fig. 1.6.

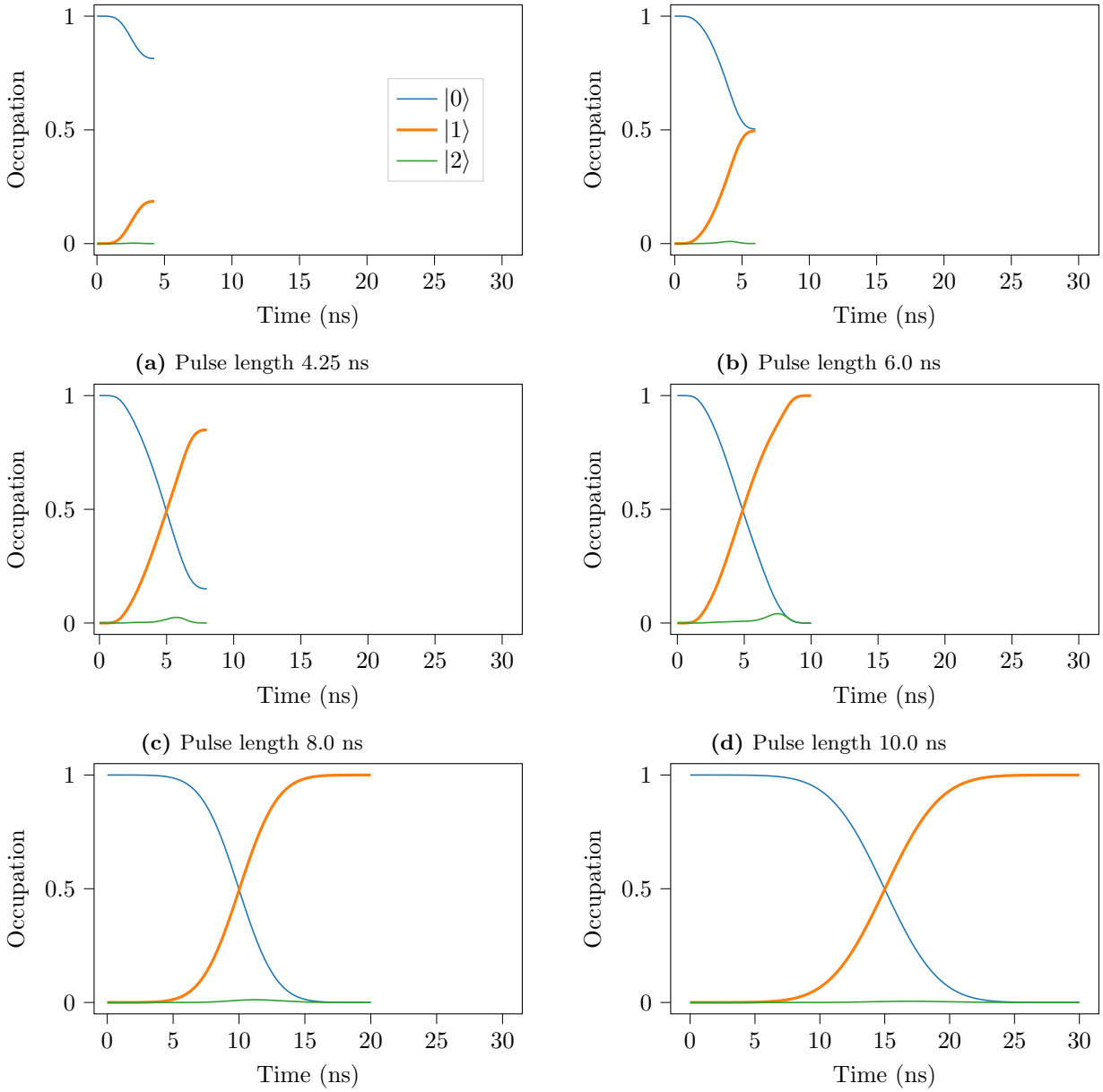

(a) Pulse length 4.25 ns

(b) Pulse length 6.0 ns

(c) Pulse length 8.0 ns

(d) Pulse length 10.0 ns

(e) Pulse length 20.0 ns

(f) Pulse length 30.0 ns

Figure 1.5: Energy level occupation over time for different lengths of optimized pulses.

For short pulse lengths there is not enough time for the transfer from $|0\rangle$ to $|1\rangle$, but for a pulse length of roughly 10.0 ns the goal is reached. Figure 1.5 **(b)** shows a little rise in occupation of $|2\rangle$ around 7.5 ns.

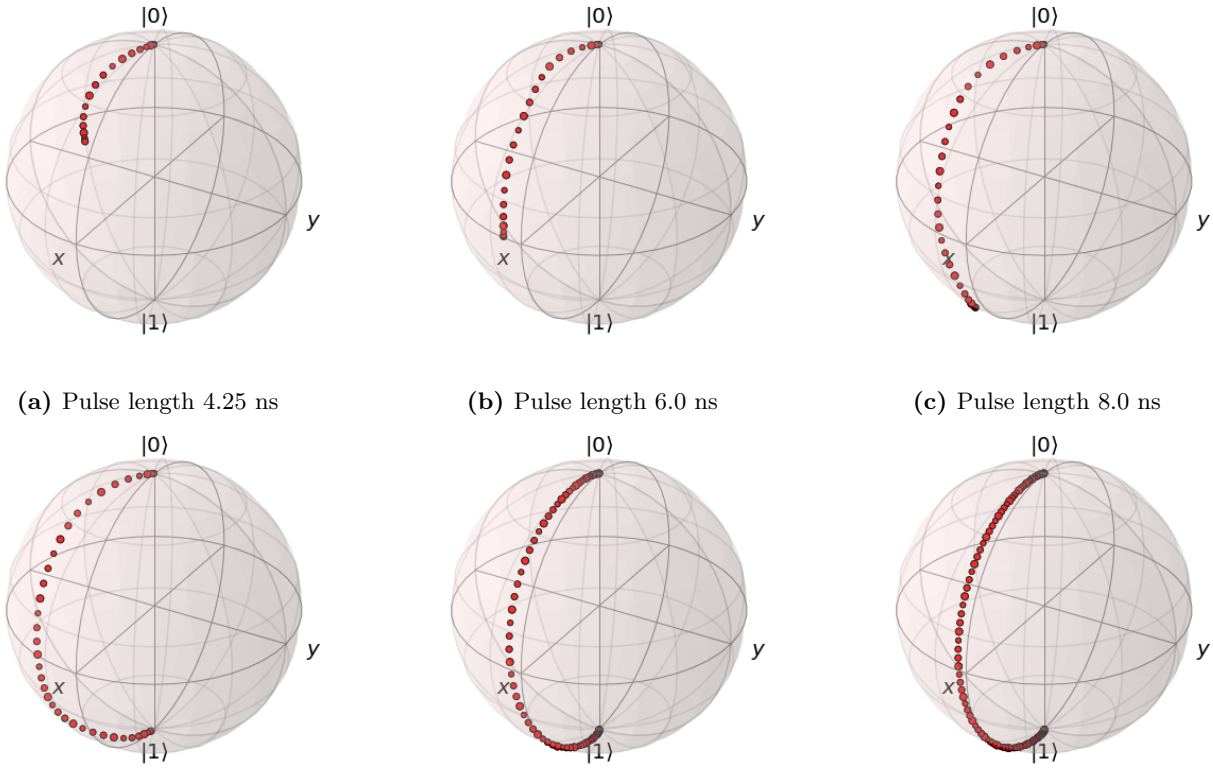

(a) Pulse length 4.25 ns **(b)** Pulse length 6.0 ns **(c)** Pulse length 8.0 ns

(d) Pulse length 10.0 ns **(e)** Pulse length 20.0 ns **(f)** Pulse length 30.0 ns

Figure 1.6: Time dynamics on the Bloch sphere for different lengths of optimized pulses.

From the Bloch sphere visualization it appears that shorter pulse lengths lead to deviations from the pure y-axis rotation. This can be clearly seen in fig. 1.6 **(d)** for a pulse length of 10 ns, where the fidelity goal was reached but short enough that the maximum amplitude is reached for the guess pulse.

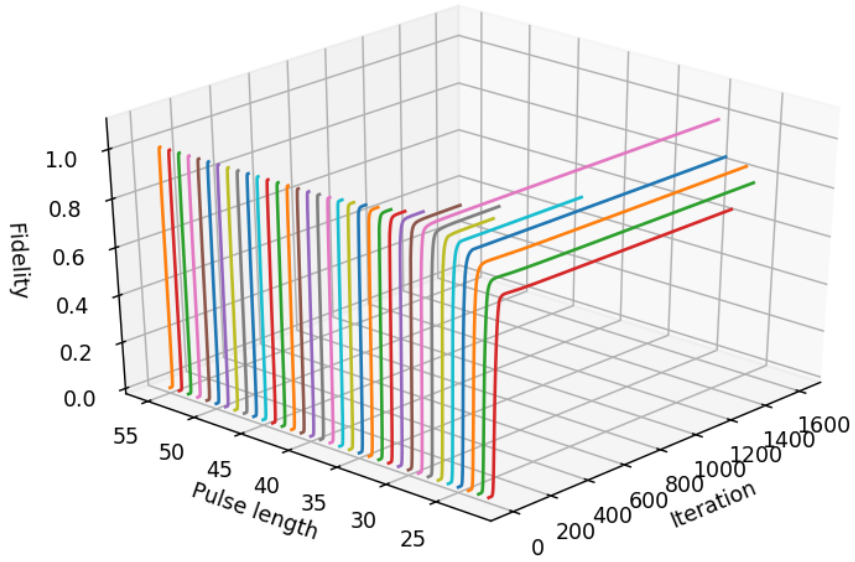

Figure 1.7: Fidelity during optimizations for every pulse length (ns).

1.1.2 $|0\rangle \rightarrow |2\rangle$ state transfer

Once again all optimization runs are shown in fig. 1.7. All runs start at almost zero fidelity while pulse lengths from 30 ns and up reach the fidelity goal of $F > 0.99999$. The number of iterations are relatively low down to 30 ns and for shorter pulses the iterations fluctuate. Note that for pulse lengths shorter than 22 ns the optimization stopped after the first iteration due to $\Delta F < 10^{-9}$.

In fig. 1.8 the fidelity is shown with respect to pulse length and here it is seen that the fidelity goal is reached for pulses down to 30 ns.

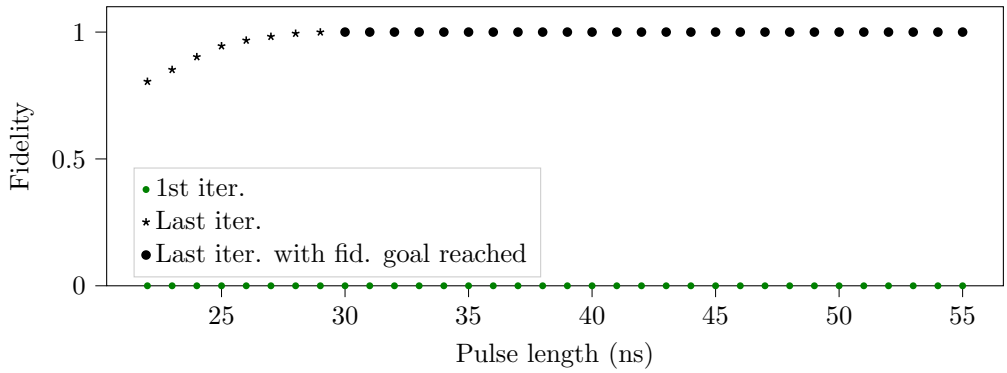

Figure 1.8: Fidelity of first and last iteration of every pulse length.

The optimized pulses are shown in fig. 1.9. For all pulse lengths the pulses have roughly the same shape with a quick rise and a short plateau, then oscillations until the end. The longest pulse at 55 ns has more oscillations than, but instead they are lower in amplitude. To get some insight, the frequency spectrum, fig. 1.10, shows large support at ω_q and $\omega_q + \kappa_q$, while for longer pulses a peak at $\omega_q - \kappa_q$ disappears. Just as the previous state transfer, the peaks narrow for longer pulse lengths.

The occupation dynamics in fig. 1.11 show a slow oscillation in all pulse lengths for all states. Further, the occupation probability of $|1\rangle$ rises to about 0.75 until the middle-point of the pulse and then falls to zero in the end, while $|2\rangle$ starts to rise at the point of the population inversion. For the shorter pulse lengths it can be seen that there isn't enough time to realise the transfer.

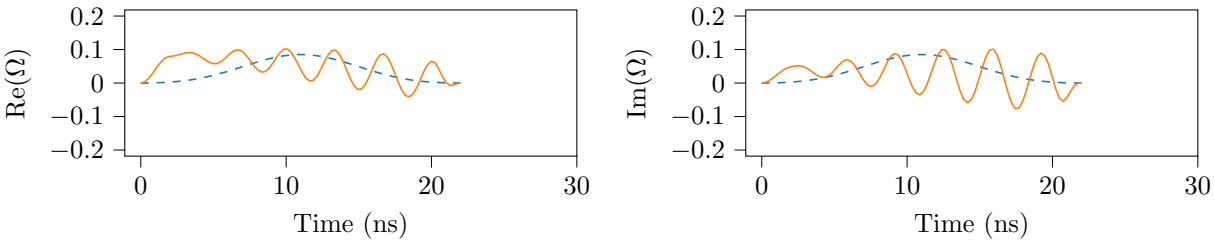

(a) Pulse length 22.0 ns

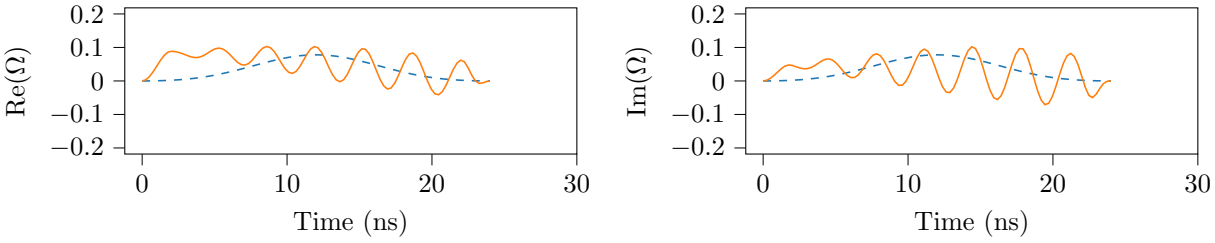

(b) Pulse length 24.0 ns

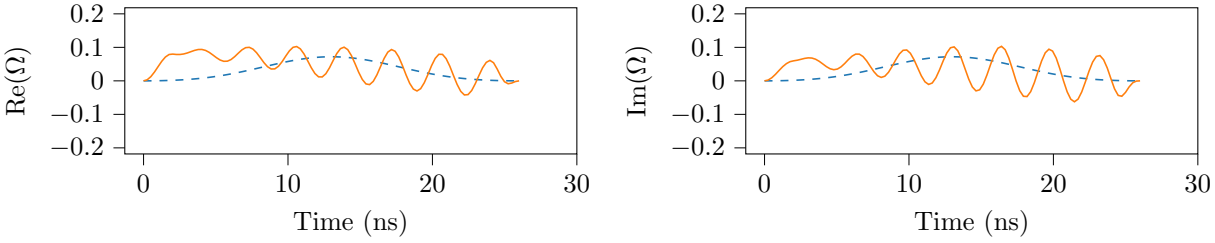

(c) Pulse length 26.0 ns

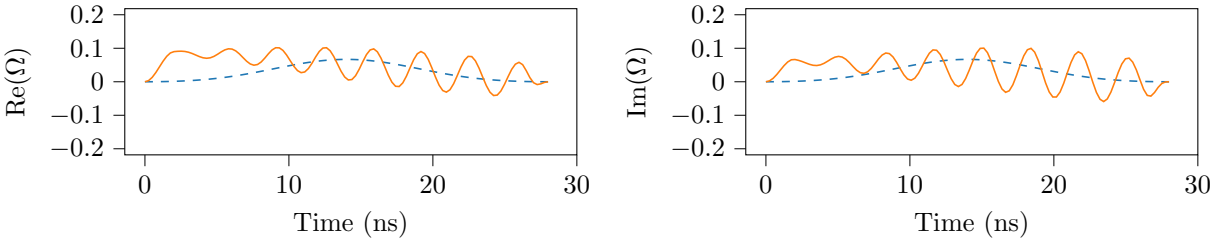

(d) Pulse length 28.0 ns

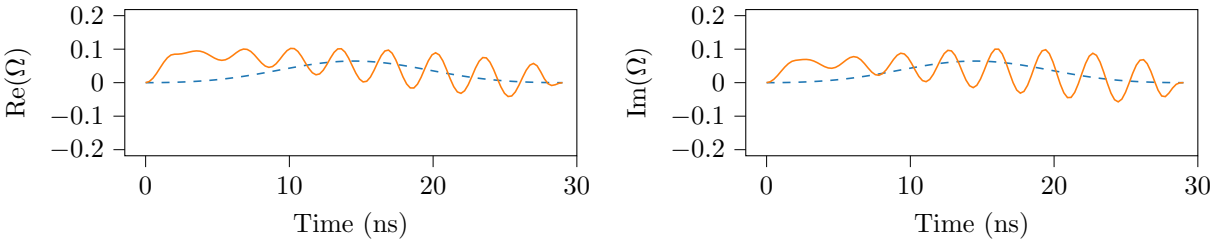

(e) Pulse length 29.0 ns

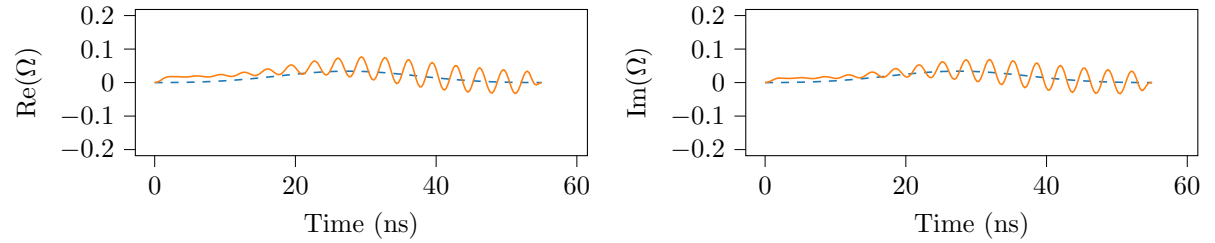

(f) Pulse length 55.0 ns

Figure 1.9: Optimised pulse shapes and guess pulses (dashed) for pulse lengths **(a)** 22 ns, **(b)** 24 ns, **(c)** 26 ns, **(d)** 28 ns, **(e)** 29 ns, and **(f)** 55 ns. Oscillations appear in all solutions.

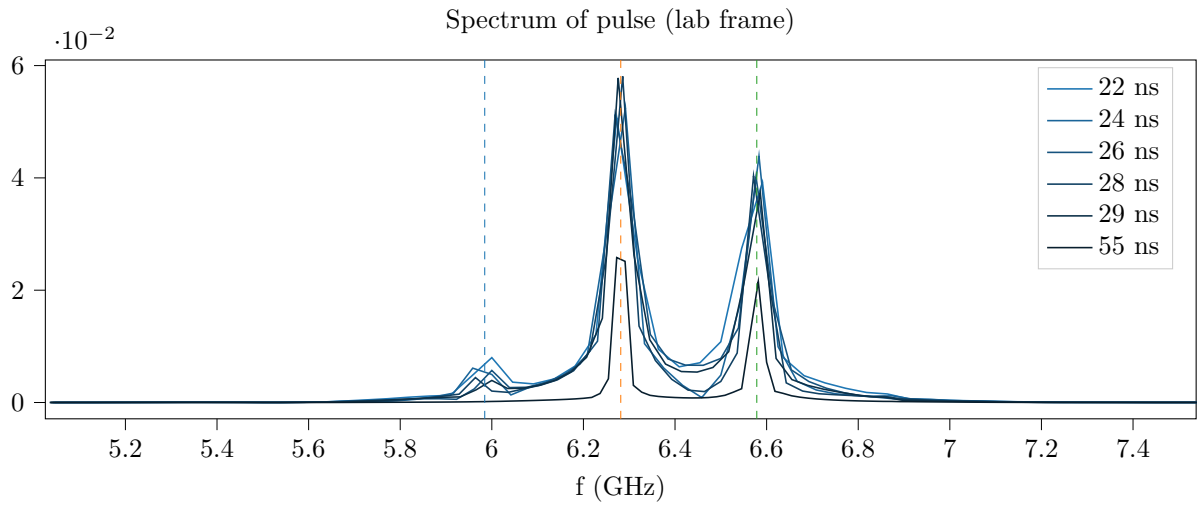

Figure 1.10: Frequency spectrum of the complex pulses in fig. 1.9. The vertical lines indicate (from left to right) $\omega_q - \kappa_q$, ω_q, $\omega_q + \kappa_q$ (all divided by 2π).

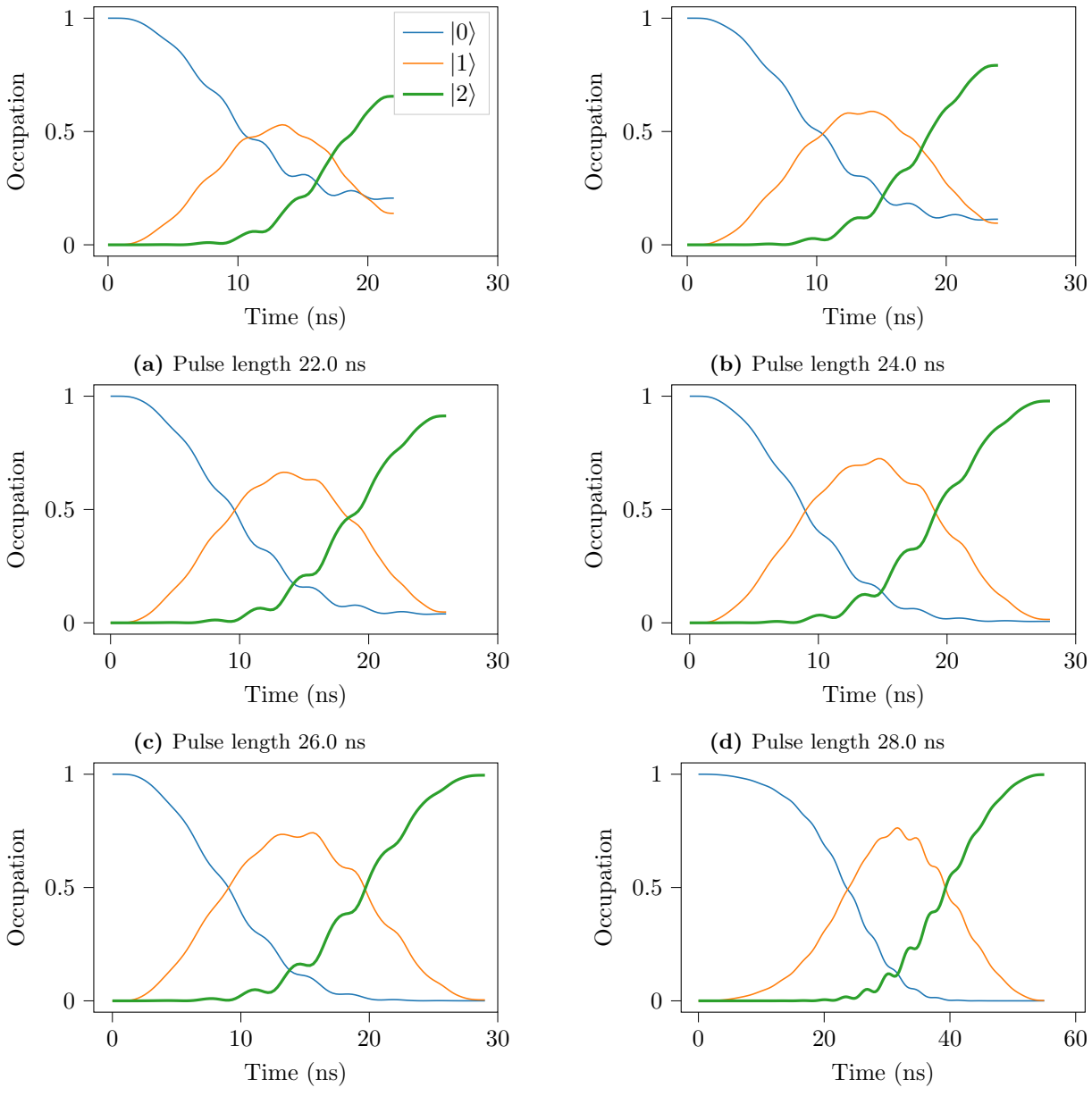

(a) Pulse length 22.0 ns

(b) Pulse length 24.0 ns

(c) Pulse length 26.0 ns

(d) Pulse length 28.0 ns

(e) Pulse length 29.0 ns

(f) Pulse length 55.0 ns

Figure 1.11: Energy level occupation over time for different lengths of optimized pulses.

1.2 Cat code encoding

The cat encoding optimization reached the convergence criteria of $\Delta F < 10^{-6}$ after 2389 iterations (totalling at roughly 41 hours and 28 minutes) with a fidelity $F = 0.999234$, (recall the fidelity measure for multiple objectives in **??**). The individual fidelities for the 6 initial states are shown in table 1.1, where we can see that all individual fidelities are above 0.999000.

Table 1.1: Fidelities for the individual state transfers (ordered from highest to lowest).

State	F
$(\|0\rangle + i\|1\rangle)/\sqrt{2}$	0.99939453
$(\|0\rangle - \|1\rangle)/\sqrt{2}$	0.99932348
$(\|0\rangle + \|1\rangle)/\sqrt{2}$	0.99930147
$\|0\rangle$	0.99920509
$\|1\rangle$	0.99918837
$(\|0\rangle - i\|1\rangle)/\sqrt{2}$	0.99899637

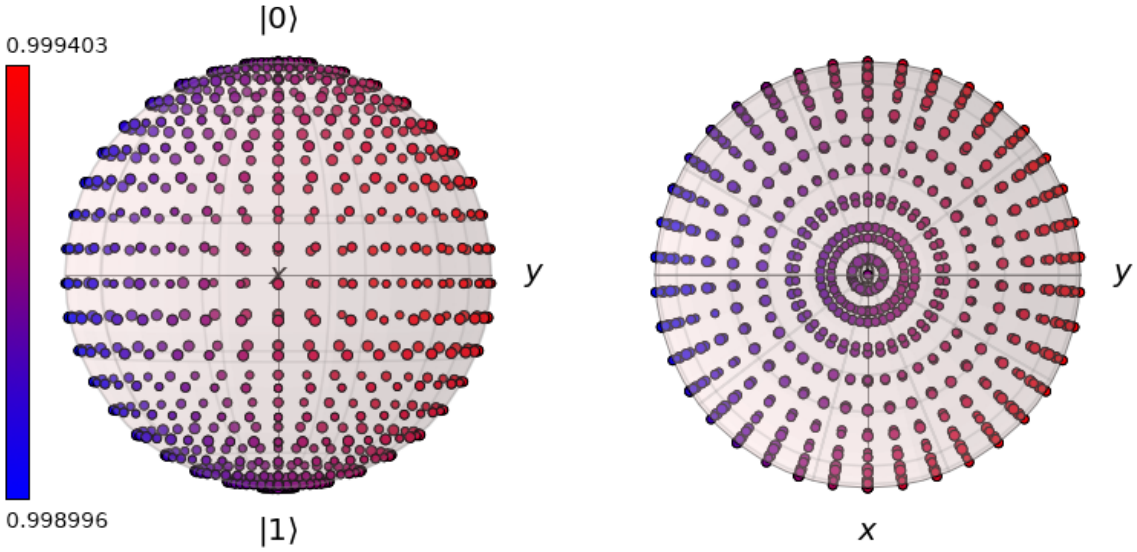

(a) Side view of Bloch sphere.

(b) Top view of Bloch sphere.

Figure 1.12: The fidelities of many simulated state transfers shown on the Bloch sphere. There is an asymmetry in the fidelity with higher fidelity towards the state $(|0\rangle + i|1\rangle)/\sqrt{2}$.

The pulse shapes of the qubit and resonator are shown in fig. 1.13. Comparing the resonator and qubit we can see that the resonator pulse has rapid oscillations throughout the whole pulse while the qubit exhibits some small quick oscillation at sparse times. The spectrum of the pulse is shown in **??** and gives us some insight into the pulse shapes. The qubit control pulse shows a wide peak at ω_q, two small peaks at ω_r and $2\omega_r - \omega_q$ and two barely noticable peaks at $\frac{1}{4}\omega_r$ and $\frac{1}{2}\omega_r$. The resonator pulse has one wide peak at ω_r, a smaller one at ω_q and an even smaller peak at $2\omega_r - \omega_q$.

The dynamics of the qubit is shown in fig. 1.15 for all state transfers. Here we see that there is always a rapid oscillation present in the occupation probability. Looking at the dynamical behaviour one can see that common for all transfers is for the qubit to stay somewhat close to an equal superposition between $|0\rangle$ and $|1\rangle$ and then at circa 50 ns evolve to $|0\rangle$.

One interesting measure we can look at is the maximum occupation of the 8 resonator states. This can give us information about the the validity of the Hilbert space truncation. In fig. 1.16 the maximum reached occupation probability are plotted for all states. This is done for all the 6 state transfers. Looking only at the odd states there is a clear downward trend for higher states, with $|7\rangle$ only reaching circa 0.2 of occupation

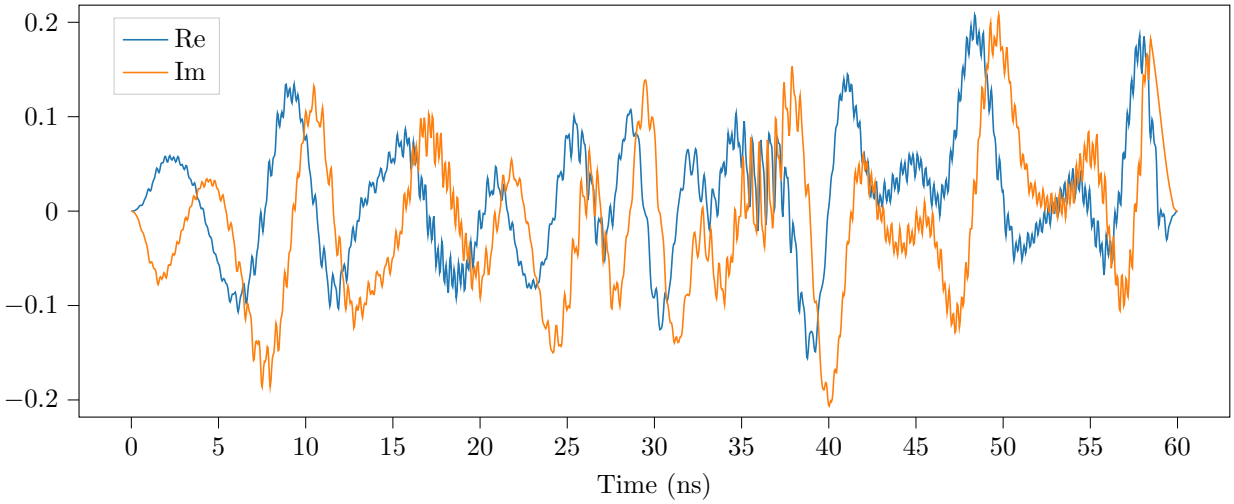

(a) Qubit control pulse shape.

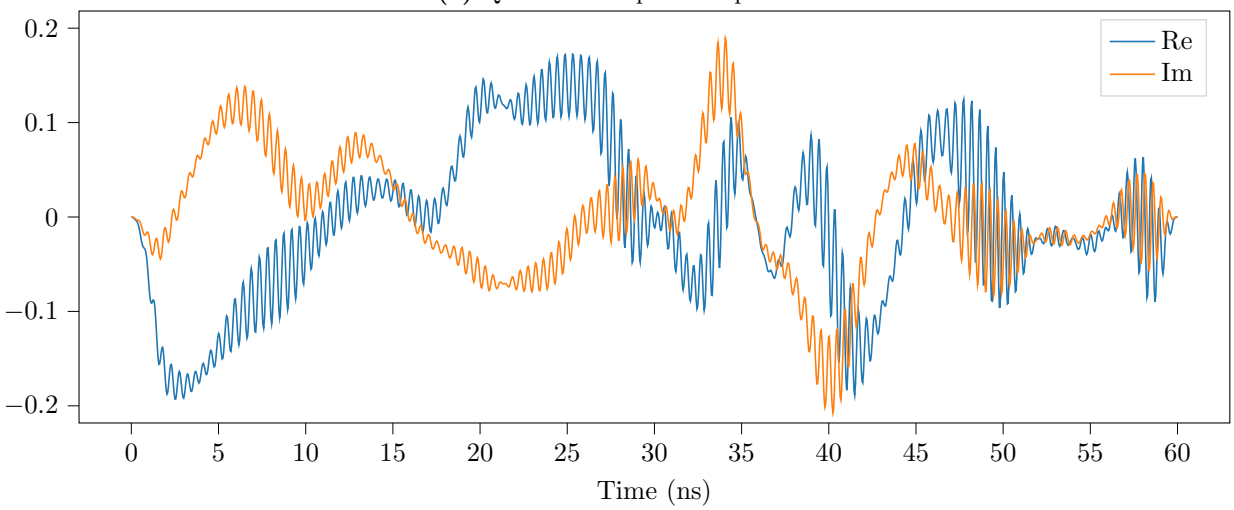

(b) Resonator control pulse shape.

Figure 1.13: Optimized pulse shapes of **(a)** $\Omega_q(t)$ and **(b)** $\Omega_r(t)$. The real and imaginary parts of the pulse are shown in blue and orange respectively. The resonator shows rapid oscillations compared to the qubit.

probability during the $|0\rangle$ transfer. $|6\rangle$ is in the 0.2–0.3 occupation range for all transfers. The dynamics of the resonator are provided in **??** for further analysis.

Finally we can plot the Wigner function of the final resonator states and compare it with the target states. This is done in fig. 1.17 where the final states have been transformed back into the lab frame. As is evident from the plots they are close to the target states shown in **??**.

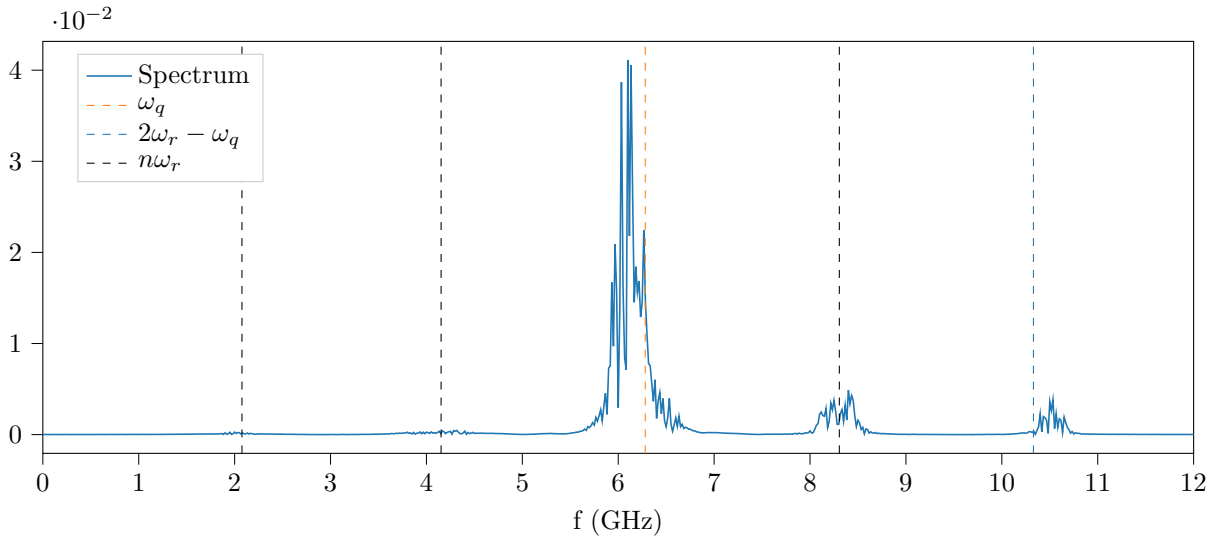

(a) Qubit control pulse spectrum. The black vertical are located at $n\omega_r$ where $n = (0.25, 0.5, 1)$.

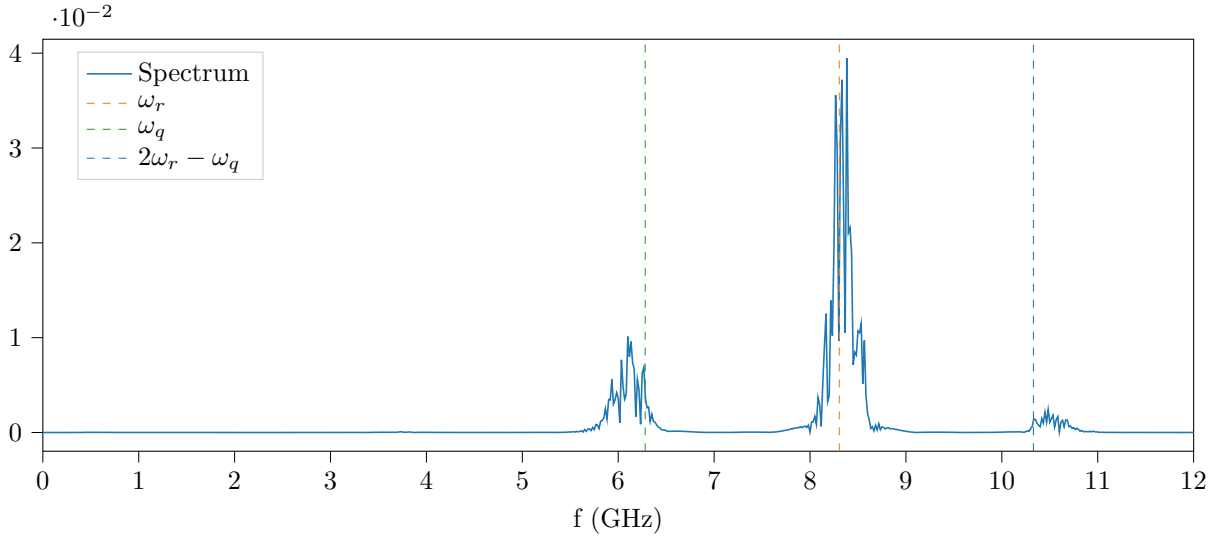

(b) Resonator control pulse spectrum.

Figure 1.14: Spectrum of optimized pulses **(a)** $\Omega_q(t)$ and **(b)** $\Omega_r(t)$ (in the lab frame).

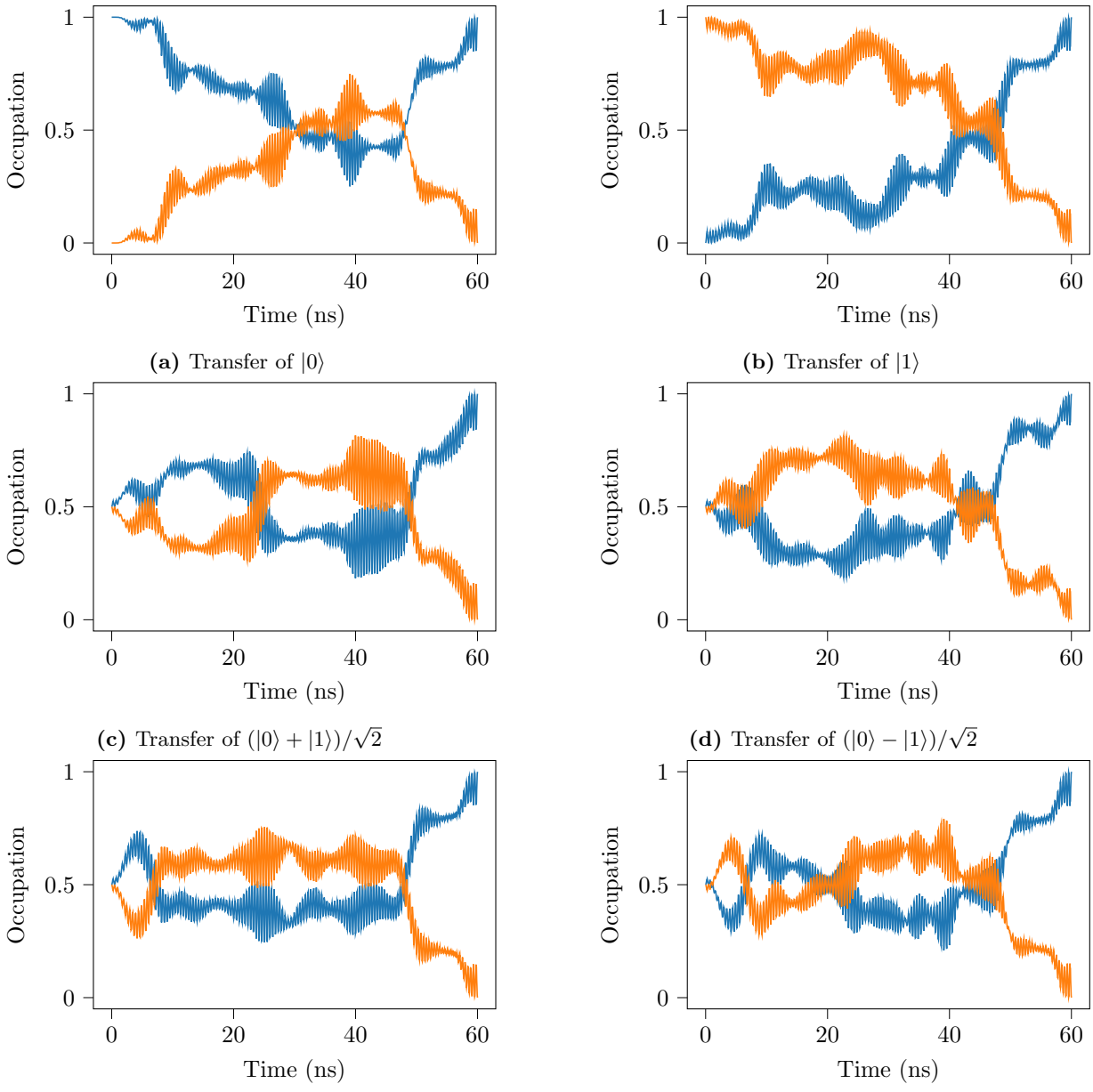

(a) Transfer of $|0\rangle$

(b) Transfer of $|1\rangle$

(c) Transfer of $(|0\rangle + |1\rangle)/\sqrt{2}$

(d) Transfer of $(|0\rangle - |1\rangle)/\sqrt{2}$

(e) Transfer of $(|0\rangle + i\,|1\rangle)/\sqrt{2}$

(f) Transfer of $(|0\rangle - i\,|1\rangle)/\sqrt{2}$

Figure 1.15: Qubit level occupation over time for the 6 state transfers. $|0\rangle$ and $|1\rangle$ are shown in blue and orange respectively.

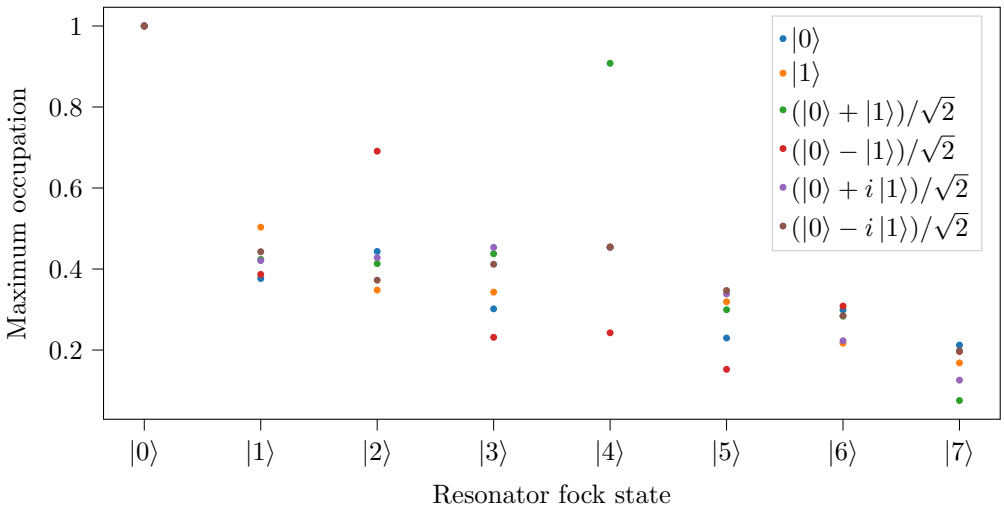

Figure 1.16: asda

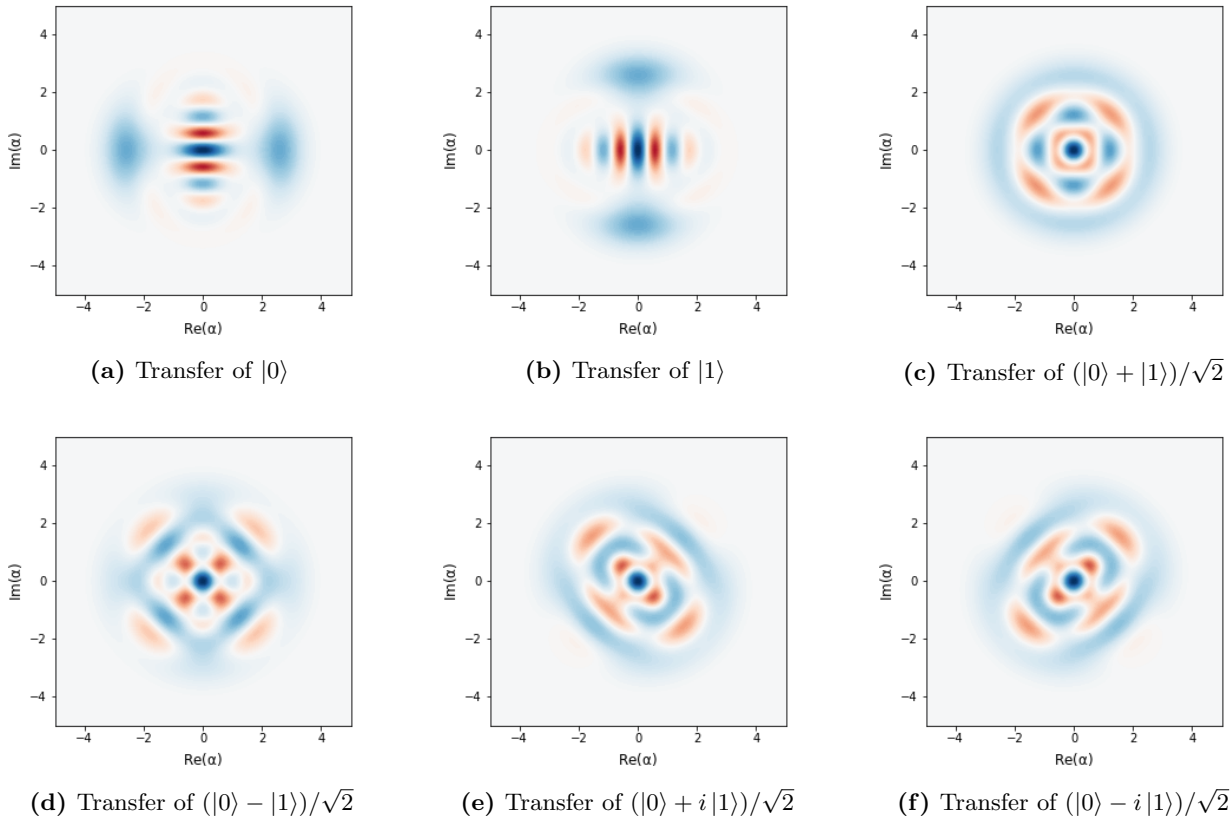

(a) Transfer of $|0\rangle$ **(b)** Transfer of $|1\rangle$ **(c)** Transfer of $(|0\rangle + |1\rangle)/\sqrt{2}$

(d) Transfer of $(|0\rangle - |1\rangle)/\sqrt{2}$ **(e)** Transfer of $(|0\rangle + i\,|1\rangle)/\sqrt{2}$ **(f)** Transfer of $(|0\rangle - i\,|1\rangle)/\sqrt{2}$

Figure 1.17: Wigner function of final state (lab frame) of the resonator for all state transfers. The final resonator states are close to the target states shown in **??**.